

000  
001  
002054  
055  
056

# Multi-channel Weighted Nuclear Norm Minimization for Real Color Image Denoising

057  
058  
059003  
004  
005  
006  
007060  
061  
062  
063

Anonymous ICCV submission

008  
009  
010  
011064  
065  
066

Paper ID 572

012  
013  
014067  
068  
069

## Abstract

015

070

The noise structures among the R, G, B channels of real images are quite different due to the preprocessing steps in digital camera pipelines. This makes the real image denoising problem much more complex than traditional grayscale image denoising. In this paper, we propose a multi-channel optimization model for real color image denoising. Specifically, we introduce a weighting matrix into the data term to process adaptively each part of R, G, B channels in the joint patches concatenated by corresponding patches in these channels. In the regularization term, we employ the weighted nuclear norm to exploit the non-local self similar property. The proposed multi-channel weighted nuclear norm minimization (MC-WNNM) model is much more complex than the standard WNNM model. To solve this new problem, we reformulate the MC-WNNM model into a linear equality-constrained problem and solve it under the alternating direction method of multipliers (ADMM) framework. Each alternative updating step has closed-form solution and the convergence results are given. Experiments on benchmark datasets demonstrate that the proposed model outperforms state-of-the-art denoising methods on synthetic as well as real-world noisy images.

038  
039071  
072

## 1. Introduction

040  
041073  
074

Image denoising is an important problem in enhancing the image quality in computer vision systems. The traditional grayscale image denoising problem aims to recover the clean image  $\mathbf{x}$  from the noisy observation  $\mathbf{y} = \mathbf{x} + \mathbf{n}$ , where  $\mathbf{n}$  is often assumed to be additive white Gaussian noise (AWGN). Most image denoising methods in this field either employ the non-local self similarity (NSS) of natural images [1–7] or learn generative or discriminative denoisers from paired natural clean images and synthetic noisy images [8–12]. Among these methods, the weighted nuclear norm minimization (WNNM) method achieves excellent denoising performance by exploiting the NSS property

via low rank regularization.

The real color image denoising problem is not a trivial extension from single channel (grayscale image) to multiple channels (color image). The reason is that the noise in standard RGB (sRGB) space, though could be modeled as AWGN, are with different variances for different channels [13] due to the on-board processing steps in digital camera pipelines [14, 15]. This makes the real color image denoising problem much more complex. Directly applying the denoising methods for grayscale images to each channel of color images separately would obtain bad performance [16]. There are several work [14, 16–20] proposed specifically for color image denoising. The method [17] first transforms the color images into the luminance/chrominance space such as YCbCr before denoising, but this would make the noise distribution more complex in color images. The methods of [16, 20] process the joint patches concatenated by the corresponding patches in R, G, B channels and treat equally the patches in different channels. This would generate false colors or artifacts [16]. The methods of [14, 18, 19] ignore the non-local self similarity property of natural images, and their performance would be largely depressed [2, 7].

In order to deal with the R, G, B channels in color images more effectively, different noise properties of different channels should be considered in solving real color image denoising problem. Besides, due to its expressive denoising performance, the WNNM model [7] is employed to exploit the NSS property of natural images. In this paper, we proposed a multi-channel WNNM (MC-WNNM) model for real color image denoising. By introducing a weighting matrix to the WNNM model, the proposed MC-WNNM model no longer has closed-form solutions and more challenging to solve. By reformulating the proposed MC-WNNM model into a linear equality-constrained program with two variables, the relaxed problem can be solved under the alternating direction method of multipliers (ADMM) [21] framework. Each variable can be updated with closed-form solution [7, 22]. We also give the convergence results with detailed proof to guarantee a rational termination of the proposed algorithm.

108  
109  
110  
111  
112  
113  
114

## 2. Related Work

### 2.1. Weighted Nuclear Norm Minimization

As an extension to the nuclear norm minimization (NNM) model [23], the weighted nuclear norm minimization (WNNM) model [7] is described as

$$\min_{\mathbf{X}} \|\mathbf{Y} - \mathbf{X}\|_F^2 + \|\mathbf{X}\|_{\mathbf{w},*} \quad (1)$$

where  $\|\mathbf{X}\|_{\mathbf{w},*} = \sum_i w_i \sigma_i(\mathbf{X})$  is the weighted nuclear norm of matrix  $\mathbf{X}$ , and  $\mathbf{w} = [w_1, \dots, w_n]^\top$ ,  $w_i \geq 0$  is the weight vector,  $\sigma_i(\mathbf{X})$  is the  $i$ -th singular value of matrix  $\mathbf{X}$ . According to the Corollary 1 of [24], the problem (1) has closed-form solution if the weights are non-decreasing

$$\hat{\mathbf{X}} = \mathbf{U} \mathcal{S}_{\mathbf{w}/2}(\Sigma) \mathbf{V}^\top \quad (2)$$

where  $\mathbf{Y} = \mathbf{U} \Sigma \mathbf{V}^\top$  is the singular value decomposition [25] of  $\mathbf{Y}$  and  $\mathcal{S}_\tau(\bullet)$  is the generalized soft-thresholding operator with weight vector  $\mathbf{w}$ :

$$\mathcal{S}_{\mathbf{w}/2}(\Sigma_{ii}) = \max(\Sigma_{ii} - w_{ii}/2, 0) \quad (3)$$

Though having achieved excellent performance on grayscale image denoising, the WNNM model would generate false colors or artifacts [16], if being directly extended to real color image denoising by processing each channel separately or joint vectors concatenated by multiple channels. In this paper, for real noisy image denoising, we propose a multi-channel WNNM model which preserve the power of WNNM and be able to process the differences among different channels.

### 2.2. Real Color Image Denoising

During the last decade, several denoising methods are proposed for real color image denoising [17–20]. Among them, the CBM3D [17] first transform the RGB image into luminance-chrominance space (e.g., YCbCr) and then apply the famous BM3D method [2] on each channel separately with the patches being grouped only in the luminance channel. In [18], the authors proposed the “Noise Level Function” to estimate and remove the noise for each channel in natural images. However, the methods processing each channel separately would achieve inferior performance than processing jointly these channels [16]. The methods of [19, 20, 26] perform real color image denoising by concatenating the patches in R, G, B channels into joint vectors. However, the concatenation would treat each channel equally and ignore the different noise properties among these channels. The method in [14] models the cross-channel noise in real noisy image as a multivariate Gaussian and the noise is removed by the Bayesian nonlocal means filter [27]. The commercial software Neat Image [28] estimates the noise parameters from a flat region of the given noisy image and filters the noise correspondingly. But

these methods [14, 28] ignore the non-local self similarity property of natural images [2, 7].

In this paper, we introduce a weighting matrix which add different weights to different channels for color image denoising. The proposed multi-channel method can effectively solve the problem of different noise structures among different channels.

## 3. Color Image Denoising via Multi-channel Weighted Nuclear Norm Minimization

### 3.1. The Problem

The color image denoising problem is to recover the clean image  $\mathbf{x}_c$  from its noisy version  $\mathbf{y}_c = \mathbf{x}_c + \mathbf{n}_c$ , where  $c = \{r, g, b\}$  is the index of R, G, B channels and  $\mathbf{n}_c$  is the noise in  $c$ -th channel. Given a noisy color image  $\mathbf{y}_c$ , each local patch of size  $p \times p \times 3$  is extracted and stretched to a patch vector  $\mathbf{y} = [\mathbf{y}_r^\top \mathbf{y}_g^\top \mathbf{y}_b^\top]^\top \in \mathbb{R}^{3p^2}$ , where  $\mathbf{y}_r, \mathbf{y}_g, \mathbf{y}_b \in \mathbb{R}^{p^2}$  are corresponding patches in R, G, B, channels. For each local patch  $\mathbf{y}$ , we search the  $M$  most similar patches to it (including  $\mathbf{y}$  itself) by Euclidean distance in a  $W \times W$  local region around it. We stack the  $M$  similar patches column by column to form a noisy patch matrix  $\mathbf{Y} = \mathbf{X} + \mathbf{N} \in \mathbb{R}^{3p^2 \times M}$ , where  $\mathbf{X}$  and  $\mathbf{N}$  the corresponding clean and noise patch matrices.

According to [13], the noise in standard RGB (sRGB) space, though could be modeled as additive white Gaussian (AWGN), are with different variances for different channels. Therefore, it is problematic to directly apply denoising methods to the joint vectors concatenated by corresponding patches of the R, G, B channels. To validate this point, in Fig. 1, we show the clean image ‘‘kodim23’’ taken from the Kodak PhotoCD dataset, its degraded version generated by adding synthetic additive white Gaussian noise (AWGN) to each channel of ‘‘kodim23’’, and the denoised image by applying WNNM [7] on the joint vectors concatenated from R, G, B channels of the degraded image. The standard derivations of AWGN added to the R, G, B channels are  $\sigma_r = 40$ ,  $\sigma_g = 20$ ,  $\sigma_b = 30$ , respectively. The input standard derivation of the noise for the concatenated WNNM method is set as the Root Mean Square (RMS) of those in each channel, i.e.,  $\sigma = \sqrt{(\sigma_r^2 + \sigma_g^2 + \sigma_b^2)/3} = 31.1$ . From Fig. 1, one can see that the concatenated WNNM method treating each channel equally would remain some noise in the R and B channel, while over-smoothing the G channel of the degraded image. Hence, if the patches of different channels are treated adaptively in the concatenated vectors, the degraded color images would be recovered with better visual qualities.

In order to process each channel differently while still exploiting the joint structures of the color images, in this paper, we introduce a weighting matrix  $\mathbf{W}$  to the concatenated

162  
163  
164  
165  
166  
167  
168  
169  
170  
171  
172  
173  
174  
175  
176  
177  
178  
179  
180  
181  
182  
183  
184  
185  
186  
187  
188  
189  
190  
191  
192  
193  
194  
195  
196  
197  
198  
199  
200  
201  
202  
203  
204  
205  
206  
207  
208  
209  
210  
211  
212  
213  
214  
215

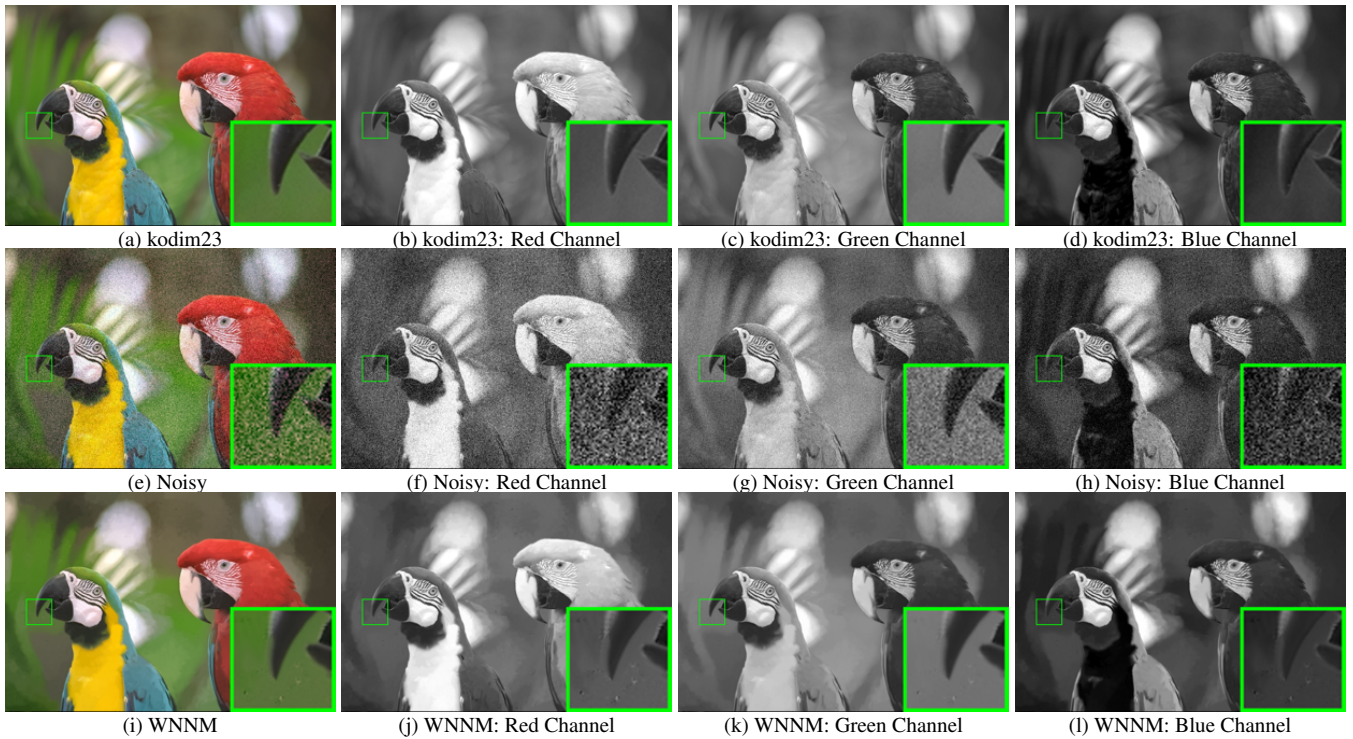


Figure 1. The image “kodim23” of the Kodak PhotoCD dataset, its degraded version, and the image recovered by WNNM. The R, G, B channels are also listed here for image quality comparison.

WNNM method. The weights  $\mathbf{w}$  for the singular values of  $\mathbf{X}$ , then the proposed multi-channel WNNM (MC-WNNM) model is

$$\min_{\mathbf{X}} \|\mathbf{W}(\mathbf{Y} - \mathbf{X})\|_F^2 + \|\mathbf{X}\|_{\mathbf{w},*}. \quad (4)$$

In [24] and this paper, the weight vector  $\mathbf{w}$  is set as  $w_i^{k+1} = \frac{C}{|\sigma_i(\mathbf{X}_k)| + \epsilon}$  where  $\epsilon > 0$  is a small number to avoid zero numerator. Note that if  $\sigma_r = \sigma_g = \sigma_b$ , the proposed MC-WNNM model will be reduced to the concatenated WNNM model as a special case. The setting of the weighting matrix  $\mathbf{W}$  and the solution of the proposed MC-WNNM model will be introduced in the next subsections.

### 3.2. The Setting of Weighting Matrix $\mathbf{W}$

For simplicity, in this paper, we assume the noise are independent among the R, G, B channels and i.i.d. in each channel. Assume the noisy patch matrix  $\mathbf{Y} = [\mathbf{Y}_r^\top \mathbf{Y}_g^\top \mathbf{Y}_b^\top]^\top$ , where  $\mathbf{Y}_r, \mathbf{Y}_g, \mathbf{Y}_b$  are matrices of similar patches in R, G, B channels, respectively. The corresponding clean matrix  $\mathbf{X} = [\mathbf{X}_r^\top \mathbf{X}_g^\top \mathbf{X}_b^\top]^\top$ , where  $\mathbf{X}_r, \mathbf{X}_g, \mathbf{X}_b$  are similarly defined. Therefore, the weighting matrix  $\mathbf{W}$  is diagonal and can be determined under the Bayesian framework:

$$\begin{aligned} \hat{\mathbf{X}} &= \arg \max_{\mathbf{X}} \ln P(\mathbf{X} | \mathbf{Y}, \mathbf{w}) \\ &= \arg \max_{\mathbf{X}} \{\ln P(\mathbf{Y} | \mathbf{X}) + \ln P(\mathbf{X} | \mathbf{w})\}. \end{aligned} \quad (5)$$

The log-likelihood term  $\ln P(\mathbf{Y} | \mathbf{X})$  is characterized by the statistics of noise, which is assumed to be channel-wise independent white Gaussian with standard deviations  $\{\sigma_r, \sigma_g, \sigma_b\}$

$$P(\mathbf{Y} | \mathbf{X}) = \prod_{c \in \{r, g, b\}} (2\pi\sigma_c^2)^{-\frac{3p^2}{2}} \exp\left(-\frac{1}{2\sigma_c^2} \|\mathbf{Y}_c - \mathbf{X}_c\|_F^2\right). \quad (6)$$

We assume that the matrix  $\mathbf{X}$  follows the following distribution

$$P(\mathbf{X} | \mathbf{w}) \propto \exp\left(-\frac{1}{2} \|\mathbf{X}\|_{\mathbf{w},*}\right). \quad (7)$$

Putting (7) and (6) into (5), we have

$$\begin{aligned} \hat{\mathbf{X}} &= \arg \min_{\mathbf{X}} \sum_{c \in \{r, g, b\}} \frac{1}{\sigma_c^2} \|(\mathbf{Y}_c - \mathbf{X}_c)\|_F^2 + \|\mathbf{X}\|_{\mathbf{w},*} \\ &= \arg \min_{\mathbf{X}} \|\mathbf{W}(\mathbf{Y} - \mathbf{X})\|_F^2 + \|\mathbf{X}\|_{\mathbf{w},*}, \end{aligned} \quad (8)$$

where

$$\mathbf{W} = \begin{pmatrix} \sigma_r^{-1} \mathbf{I} & \mathbf{0} & \mathbf{0} \\ \mathbf{0} & \sigma_g^{-1} \mathbf{I} & \mathbf{0} \\ \mathbf{0} & \mathbf{0} & \sigma_b^{-1} \mathbf{I} \end{pmatrix}. \quad (9)$$

where  $\mathbf{I} \in \mathbb{R}^{p^2 \times p^2}$  is the identity matrix. Hence, the weighting matrix  $\mathbf{W}$  is determined to contribute equal weights for the pixel values in the same channel, while different weights for those in different channels. The experimental (which will be introduced later) results have already demonstrated

324 that this form of weighting matrix have already generated  
 325 the best denoising performance on synthetic and real noisy  
 326 images in benchmark datasets.  
 327

### 328 3.3. Optimization

329 The proposed MC-WNNM model could not be solved in  
 330 an analytical form while the original WNNM model  
 331 [24] could. In the WNNM model, when the weights on  
 332 singular values are non-descending, the weighted nuclear  
 333 norm proximal operator [24] can have global optimum with  
 334 closed-form solution. However, such property is not valid  
 335 for the multi-channel WNNM model. The reason is that the  
 336 weighting matrix  $\mathbf{W}$  is added to the rows of matrix  $\mathbf{X}$  instead  
 337 of its singular values. Besides, the elements in  $\mathbf{W}$  is  
 338 not in a non-descending order with respect to the singular  
 339 value of  $\mathbf{X}$ . This makes the proposed model more difficult  
 340 to solve when compared to the original WNNM model.  
 341

342 By introducing an augmented variable  $\mathbf{Z}$ , the MC-  
 343 WNNM model is reformulated as a linear equality-  
 344 constrained problem with two variables  $\mathbf{X}$  and  $\mathbf{Z}$ :

$$345 \min_{\mathbf{X}, \mathbf{Z}} \|\mathbf{W}(\mathbf{Y} - \mathbf{X})\|_F^2 + \|\mathbf{Z}\|_{w,*} \quad \text{s.t.} \quad \mathbf{X} = \mathbf{Z}. \quad (10)$$

347 Since the objective function is separable across the two vari-  
 348 ables, the problem (10) can be solved under alternating di-  
 349 rection method of multipliers (ADMM) framework. We can  
 350 derive its augmented Lagrangian function:  
 351

$$352 \mathcal{L}(\mathbf{X}, \mathbf{Z}, \mathbf{A}, \rho) = \|\mathbf{W}(\mathbf{Y} - \mathbf{X})\|_F^2 + \|\mathbf{Z}\|_{w,*} \\ 353 \quad + \langle \mathbf{A}, \mathbf{X} - \mathbf{Z} \rangle + \frac{\rho}{2} \|\mathbf{X} - \mathbf{Z}\|_F^2 \quad (11)$$

355 where  $\mathbf{A}$  is the augmented Lagrangian multiplier and  $\rho > 0$   
 356 is the penalty parameter. We initialize the matrix variables  
 357  $\mathbf{X}_0$ ,  $\mathbf{Z}_0$ , and  $\mathbf{A}_0$  to be zero matrix of suitable size. By tak-  
 358 ing derivative of the Lagrangian function  $\mathcal{L}$  with respect to  
 359 the variables  $\mathbf{X}$  and  $\mathbf{Z}$  and setting the derivative function to  
 360 be zero, we can alternatively update the ADMM algorithm  
 361 iteratively as follows:

362 (1) **Update  $\mathbf{X}$  while fixing  $\mathbf{Z}$  and  $\mathbf{A}$ :**

$$364 \mathbf{X}_{k+1} = \arg \min_{\mathbf{X}} \|\mathbf{W}(\mathbf{Y} - \mathbf{X})\|_F^2 + \frac{\rho_k}{2} \|\mathbf{X} - \mathbf{Z}_k + \rho_k^{-1} \mathbf{A}_k\|_F^2 \\ 365 \quad (12)$$

366 This is a standard least squares regression problem with  
 367 closed-form solution:

$$369 \mathbf{X}_{k+1} = (\mathbf{W}^\top \mathbf{W} + \frac{\rho_k}{2} \mathbf{I})^{-1} (\mathbf{W}^\top \mathbf{W} \mathbf{Y} + \frac{\rho_k}{2} \mathbf{Z}_k - \frac{1}{2} \mathbf{A}_k) \\ 370 \quad (13)$$

372 (2) **Update  $\mathbf{Z}$  while fixing  $\mathbf{X}$  and  $\mathbf{A}$ :**

$$374 \mathbf{Z}_{k+1} = \arg \min_{\mathbf{Z}} \frac{\rho_k}{2} \|\mathbf{Z} - (\mathbf{X}_{k+1} + \rho_k^{-1} \mathbf{A}_k)\|_F^2 + \|\mathbf{Z}\|_{w,*} \\ 375 \quad (14)$$

376 According to the Theorem 1 in [24], given the  $\mathbf{X}_{k+1} +$   
 377  $\rho_k^{-1} \mathbf{A}_k = \mathbf{U}_k \Sigma_k \mathbf{V}_k^\top$  be the SVD of  $\mathbf{X}_{k+1} + \rho_k^{-1} \mathbf{A}_k$ ,

378 where  $\Sigma_k = \begin{pmatrix} \text{diag}(\sigma_1, \sigma_2, \dots, \sigma_n) \\ \mathbf{0} \end{pmatrix} \in \mathbb{R}^{m \times n}$ , then the  
 379 global optimum of the above problem is  $\hat{\mathbf{Z}} = \mathbf{U}_k \hat{\Sigma}_k \mathbf{V}_k^\top$ ,  
 380 where  $\hat{\Sigma}_k = \begin{pmatrix} \text{diag}(\hat{\sigma}_1, \hat{\sigma}_2, \dots, \hat{\sigma}_n) \\ \mathbf{0} \end{pmatrix} \in \mathbb{R}^{m \times n}$  and  
 381  $(\hat{\sigma}_1, \hat{\sigma}_2, \dots, \hat{\sigma}_n)$  is the solution to the following convex opti-  
 382 mization problem:  
 383

$$386 \min_{\hat{\sigma}_1, \hat{\sigma}_2, \dots, \hat{\sigma}_n} \sum_{i=1}^n (\sigma_i - \hat{\sigma}_i)^2 + \frac{2w_i}{\rho_k} \hat{\sigma}_i \\ 387 \quad \text{s.t.} \quad \hat{\sigma}_1 \geq \hat{\sigma}_2 \geq \dots \geq \hat{\sigma}_n \geq 0. \\ 388 \quad (389)$$

390 According to the Remark 1 in [24], the problem above has  
 391 closed-form solution

$$393 \hat{\sigma}_i = \begin{cases} 0 & \text{if } c_2 < 0 \\ \frac{c_1 + \sqrt{c_2}}{2} & \text{if } c_2 \geq 0 \end{cases} \quad (394)$$

395 where  $c_1 = \sigma_i - \epsilon$ ,  $c_2 = (\sigma_i - \epsilon)^2 - \frac{8C}{\rho_k}$  and  $C$  is set as  
 396  $\sqrt{2M}$  by experience in image denoising.

397 (3) **Update  $\mathbf{A}$  while fixing  $\mathbf{X}$  and  $\mathbf{Z}$ :**

$$399 \mathbf{A}_{k+1} = \mathbf{A}_k + \rho_k (\mathbf{X}_{k+1} - \mathbf{Z}_{k+1}) \quad (400)$$

401 (4) **Update  $\rho_k$ :**  $\rho_{k+1} = \mu * \rho_k$ , where  $\mu > 1$ .

402 The above alternative updating steps are repeated until  
 403 the convergence condition is satisfied or the number of  
 404 iterations exceeds a preset maximum number, e.g.,  $K_1$ .  
 405 The convergence condition of the ADMM algorithm is:  
 406  $\|\mathbf{X}_{k+1} - \mathbf{Z}_{k+1}\|_F \leq \text{Tol}$ ,  $\|\mathbf{X}_{k+1} - \mathbf{X}_k\|_F \leq \text{Tol}$ , and  
 407  $\|\mathbf{Z}_{k+1} - \mathbf{Z}_k\|_F \leq \text{Tol}$  are simultaneously satisfied, where  
 408  $\text{Tol} > 0$  is a small tolerance. We summarize the updating  
 409 steps in Algorithm 1. The convergence analysis of the pro-  
 410 posed Algorithm 1 is given in Theorem 1. Note that since  
 411 the weighted nuclear norm is non-convex in general, we em-  
 412 ploy an unbounded sequence of  $\{\rho_k\}$  here to make sure that  
 413 the Algorithm 1 is convergent.

414 **Theorem 1.** Assume the weights in  $w$  are in a non-  
 415 descending order, the sequence  $\{\mathbf{X}_k\}$ ,  $\{\mathbf{Z}_k\}$ , and  $\{\mathbf{A}_k\}$   
 416 generated in Algorithm 1 satisfy:

$$418 (a) \lim_{k \rightarrow \infty} \|\mathbf{X}_{k+1} - \mathbf{Z}_{k+1}\|_F = 0; \quad (419)$$

$$420 (b) \lim_{k \rightarrow \infty} \|\mathbf{X}_{k+1} - \mathbf{X}_k\|_F = 0; \quad (421)$$

$$422 (c) \lim_{k \rightarrow \infty} \|\mathbf{Z}_{k+1} - \mathbf{Z}_k\|_F = 0. \quad (423)$$

424 *Proof.* We give proof sketch here and detailed proof of  
 425 this theorem can be found in supplementary files. We  
 426 can first proof that the sequence  $\{\mathbf{A}_k\}$  generated by Algo-  
 427 rithm 1 is upper bounded. Since  $\{\rho_k\}$  is unbounded, that  
 428 is  $\lim_{k \rightarrow \infty} \rho_k = +\infty$ , we can proof that the sequence  
 429 of Lagrangian function  $\{\mathcal{L}(\mathbf{X}_{k+1}, \mathbf{Z}_{k+1}, \mathbf{A}_k, \rho_k)\}$  is also  
 430 upper bounded. Hence, both  $\{\mathbf{W}(\mathbf{Y} - \mathbf{X}_k)\}$  and  $\{\mathbf{Z}_k\}$   
 431 are upper bounded. According to Eq. (17), we can proof

**Algorithm 1:** Solve MC-WNNM via ADMM

---

**Input:** Matrices  $\mathbf{Y}$  and  $\mathbf{W}$ ,  $\mu > 1$ ,  $\text{Tol} > 0$ ;

**Initialization:**  $\mathbf{X}_0 = \mathbf{Z}_0 = \mathbf{A}_0 = \mathbf{0}$ ,  $\rho_0 > 0$ ,  $\mathbf{T} = \text{False}$ ,  $k = 0$ ;

**While** ( $\mathbf{T} == \text{false}$ ) **do**

1. Update  $\mathbf{X}_{k+1}$  as  

$$\mathbf{X}_{k+1} = (\mathbf{W}^\top \mathbf{W} + \frac{\rho_k}{2} \mathbf{I})^{-1} (\mathbf{W}^\top \mathbf{W} \mathbf{Y} + \frac{\rho_k}{2} \mathbf{Z}_k - \frac{1}{2} \mathbf{A}_k)$$
2. Update  $\mathbf{Z}_{k+1}$  by solving the problem  

$$\min_{\mathbf{Z}} \frac{\rho_k}{2} \|\mathbf{Z}\|_F^2 + \|\mathbf{Z}\|_{w,*}$$
3. Update  $\mathbf{A}_{k+1}$  as  $\mathbf{A}_{k+1} = \mathbf{A}_k + \rho_k (\mathbf{X}_{k+1} - \mathbf{Z}_{k+1})$
4. Update  $\rho_{k+1} = \mu * \rho_k$ ;
5.  $k \leftarrow k + 1$ ;  
**if** (Convergence condition is satisfied) or ( $k \geq K_1$ )  
5.  $\mathbf{T} \leftarrow \text{True}$   
**end if**  
**end while**

**Output:** Matrices  $\mathbf{X}$  and  $\mathbf{Z}$ .

---

that  $\lim_{k \rightarrow \infty} \|\mathbf{X}_{k+1} - \mathbf{Z}_{k+1}\|_F = \lim_{k \rightarrow \infty} \rho_k^{-1} \|\mathbf{A}_{k+1} - \mathbf{A}_k\|_F = 0$ , and (a) is proofed. Then we can proof that  $\lim_{k \rightarrow \infty} \|\mathbf{X}_{k+1} - \mathbf{X}_k\|_F \leq \lim_{k \rightarrow \infty} \|(\mathbf{W}^\top \mathbf{W} + \frac{\rho_k}{2} \mathbf{I})^{-1} (\mathbf{W}^\top \mathbf{W} \mathbf{Y} - \mathbf{W}^\top \mathbf{W} \mathbf{Z}_k - \frac{1}{2} \mathbf{A}_k)\|_F + \rho_k^{-1} \|\mathbf{A}_k - \mathbf{A}_{k-1}\|_F = 0$  and hence (b) is proofed. Then (c) can be proofed by checking that  $\lim_{k \rightarrow \infty} \|\mathbf{Z}_{k+1} - \mathbf{Z}_k\| \leq \lim_{k \rightarrow \infty} \|\Sigma_{k-1} - \mathcal{S}_{w/\rho_{k-1}}(\Sigma_{k-1})\|_F + \|\mathbf{X}_{k+1} - \mathbf{X}_k\|_F + \rho_k^{-1} \|\mathbf{A}_{k-1} + \mathbf{A}_{k+1} - \mathbf{A}_k\|_F = 0$ , where  $\mathbf{U}_{k-1} \Sigma_{k-1} \mathbf{V}_{k-1}^\top$  is the SVD of the matrix  $\mathbf{X}_k + \rho_{k-1} \mathbf{A}_{k-1}$ .  $\square$

### 3.4. The Denoising Algorithm

Given a noisy color image  $\mathbf{y}_c$ , assume we have extracted  $N$  local patches  $\{\mathbf{y}_j\}_{j=1}^N$  and corresponding similar patches to form the noisy patch matrices  $\{\mathbf{Y}_j\}_{j=1}^N$ . The proposed MC-WNNM is applied to the noisy patch matrix  $\mathbf{Y}_j$  of each local patch  $\mathbf{y}_j$  ( $j = 1, \dots, N$ ) of the noisy image  $\mathbf{y}_c$ . And then all the estimated clean patch matrices  $\{\mathbf{X}_j\}_{j=1}^N$  are aggregated together to form the final recovered image  $\hat{\mathbf{x}}_c$ . To obtain better denoising results, we perform the above denoising procedure for several ( $K_2$ ) iterations. The proposed MC-WNNM denoising algorithm for color images is summarized in Algorithm 2.

## 4. Experiments

We evaluate the proposed MC-WNNM method on synthetic and real color image denoising. We compare the proposed method with other state-of-the-art denoising methods including CBM3D [17], MLP [10], WNNM [7], TNRD [12], “Noise Clinic” (NC) [19, 26], and the commercial software Neat Image (NI) [28].

### 4.1. Implementation Details

In synthetic experiments, the noise levels in R, G, B channels are assumed to be known as  $\sigma_r, \sigma_g, \sigma_b$ . In the real

**Algorithm 2:** Color Image Denoising by MC-WNNM

---

**Input:** Noisy image  $\mathbf{y}_c$ , noise levels  $\{\sigma_r, \sigma_g, \sigma_b\}$ ;

**Initialization:**  $\hat{\mathbf{x}}_c^{(0)} = \mathbf{y}_c$ ,  $\mathbf{y}_c^{(0)} = \mathbf{y}_c$ ;

**for**  $k = 1 : K_2$  **do**

1. Set  $\mathbf{y}_c^{(k)} = \hat{\mathbf{x}}_c^{(k-1)}$ ;
2. Extract local patches  $\{\mathbf{y}_j\}_{j=1}^N$  from  $\mathbf{y}_c^{(k)}$ ;  
**for** each patch  $\mathbf{y}_j$  **do**
3. Search non-local similar patches  $\mathbf{Y}_j$ ;
4. Apply the MC-WNNM model (10) to  $\mathbf{Y}_j$  and obtain the estimated  $\mathbf{X}_j$ ;

**end for**

5. Aggregate  $\{\mathbf{X}_j\}_{j=1}^N$  to form the image  $\hat{\mathbf{x}}_c^{(k)}$ ;

**end for**

**Output:** Denoised image  $\hat{\mathbf{x}}_c^{K_2}$ .

---

cases, the noise levels in R, G, B channels can be estimated via noise estimation methods [29, 30]. In this paper, we employ the method of [30] for its state-of-the-art performance. For the CBM3D method [17], the input noise levels are the Root Mean Square (RMS) as

$$\sigma = \sqrt{(\sigma_r^2 + \sigma_g^2 + \sigma_b^2)/3}. \quad (21)$$

For the methods of MLP [10] and TNRD [12], we retrain the models on grayscale images following their corresponding strategies at different noise levels from  $\sigma = 5$  to  $\sigma = 75$  with gap of 5. The denoising on color images is performed by processing separately each channel with the model trained at the same (or nearest) noise levels. NC [19, 26] is a blind image denoising method, so we just submit the noisy images (synthetic or real) to [26] and perform denoising using the default parameters. NI [28] is a commercial software suitable for real image denoising, while the code of CC [14] is not released (but its results on the 15 real noisy images in [14] are available by requesting the authors). Hence, we only compare with CC and NI in real image denoising experiments, and do not compare with them in synthetic experiments.

In order to take fully comparison with the original WNNM method [24], we extended the WNNM method [24] for color image denoising in three directions: 1) we apply the WNNM method [24] on each channel separately with corresponding noise levels  $\sigma_r, \sigma_g, \sigma_b$ . We call this method “WNNM0”; 2) we perform denoising on the joint vectors concatenated by corresponding patches in the R, G, B channels, where the input noise level  $\sigma$  is computed by RMS (Eq. (21)). We call this method “WNNM1”; 3) we set the weighting matrix  $\mathbf{W}$  in the proposed MC-WNNM model as  $\mathbf{W} = \sigma^{-1} \mathbf{I}$ . For fair comparison, we tune all these methods set the same parameters for “WNNM2” and the proposed MC-WNNM methods while achieving the best performance of “WNNM2”. For fair comparison, we tune the methods of “WNNM0”, “WNNM1”, “WNNM2”, and the proposed

540 MC-WNNM to achieve corresponding best denoising per-  
 541 formance (i.e., highest average PSNR results).  
 542  
 543  
 544

## 4.2. Experiments on Synthetic Noisy Images

547 In this section, we compare the proposed MC-WNNM  
 548 method with other competing denoising methods [10, 12,  
 549 17, 19, 28] as well as the three extensions of the original  
 550 WNNM method [24] on the 24 high quality color images from  
 551 the Kodak PhotoCD Dataset (<http://r0k.us/graphics/kodak/>), which are shown in Fig. 2.  
 552 The noisy images are generated by adding additive white  
 553 Gaussian noise (AWGN) with known standard derivations  
 554  $\sigma_r, \sigma_g, \sigma_b$  for the R, G, B channels, respectively. In this  
 555 paper, the noise levels we add to each channel of the 24  
 556 color images are  $\sigma_r = 40, \sigma_g = 20, \sigma_b = 30$ , respectively.  
 557 More experiments can be found in the supplementary files.  
 558 For the methods of “WNNM2” and MC-WNNM, we set the  
 559 patch size as  $p = 6$ , the number of non-local similar patches  
 560 as  $M = 70$ , the window size for searching similar patches  
 561 as  $W = 20$ , the updating parameter  $\mu = 1.001$ , the num-  
 562 ber of iterations in Algorithm 1 as  $K_1 = 8$ , the number of  
 563 iterations in Algorithm 2 as  $K_2 = 10$ . For “WNNM2”, the  
 564 initial penalty parameter is set as  $\rho_0 = 10$ , while for the  
 565 proposed MC-WNNM model, the penalty parameter is set  
 566 as  $\rho_0 = 3$ .  
 567

568 The PSNR results are listed in Table 1 of the com-  
 569 pared methods including CBM3D [17], MLP [10], TNRD  
 570 [12], NI [28], NC [19, 26], “WNNM0” [24], “WNNM1”,  
 571 “WNNM2” and the proposed MC-WNNM methods. The  
 572 best PSNR results are highlighted in bold. One can see that  
 573 on all the 24 images, our method achieves the highest PSNR  
 574 values over the competing methods. On average PSNR,  
 575 our proposed method achieves 0.48dB improvements over  
 576 the “WNNM0” method and outperforms the “WNNM2”  
 577 by 1.09dB. Fig. 3 shows a scene denoised by the  
 578 compared methods. We can see that the methods of CBM3D  
 579 and NC would remain some noise on the recovered images.  
 580 The methods of MLP, TNRD, and “WNNM0”, which  
 581 process separately the channels of color images, would  
 582 over-smooth the images and generate false colors or artifacts.  
 583 The method “WNNM1”, which process jointly the chan-  
 584 nels of color images, would not generate false colors, but  
 585 still over-smooth the image. The “WNNM2”, which is the  
 586 WNNM model solved by ADMM algorithm, would remain  
 587 some noise on the image. By employing the proposed MC-  
 588 WNNM model, our method preserves the structures (e.g.,  
 589 textures in windows and grass) better across the R, G, B  
 590 channels and generate less artifacts than other denoising  
 591 methods, leading to visually pleasant outputs. More visual  
 592 comparisons can be found in the supplementary files.  
 593



Figure 2. The 24 high quality color images from the Kodak PhotoCD Dataset.

## 4.3. Experiments on Real Noisy Images

594 In this section, we compare the proposed MC-WNNM  
 595 method with other competing methods on the 15 real noisy  
 596 images (Fig. 4). We do not compare with the “WNNM0”  
 597 method due to limited space and its inferior performance.  
 598 The noisy images were collected under controlled indoor  
 599 environment. Each scene was shot 500 times under the same  
 600 camera and camera setting. The mean image of the 500  
 601 shots is roughly taken as the “ground truth”, with which the  
 602 PSNR can be computed. Since the image size is very large  
 603 (about  $7000 \times 5000$ ) and the 11 scenes share repetitive con-  
 604 tents, the authors of [14] cropped 15 smaller images (of size  
 605  $512 \times 512$ ) to perform experiments. For each real noisy im-  
 606 age, the noise levels in R, G, B channels are estimated by  
 607 [30]. Since the noise levels are small in real noisy images,  
 608 for the method of MLP [10] and TNRD [12], we apply the  
 609 trained models of corresponding methods and choose the  
 610 best denoising results (highest average PSNR values). Both  
 611 methods achieves best results when setting the noise levels  
 612 of the trained models from  $\sigma = 10$ .

613 We perform quantitative comparison on the 15 cropped  
 614 images used in [14]. The PSNR results are listed in Ta-  
 615 ble 2 of the compared methods including CBM3D [17],  
 616 MLP [10], TNRD [12], NC [19, 26], NI [28], CC [14]  
 617 (copied from [14]), “WNNM1”, “WNNM2”, and the pro-  
 618 posed MC-WNNM method. The highest PSNR results are  
 619 highlighted in bold. On average PSNR, the proposed MC-  
 620 WNNM method achieves 0.44dB improvements over the  
 621 “WNNM1” method and outperforms the state-of-the-art de-  
 622 noising method CC [14] by 0.83dB. On 10 out of the whole  
 623 15 images, the proposed MC-WNNM method achieves the  
 624 highest PSNR values. Both CC and “WNNM1” achieves  
 625 highest PSNR results on 2 of 15 images. It should be noted  
 626 that in the CC method, a specific model is trained for each  
 627 camera and camera setting, while our method uses the same  
 628 model for all cases. Fig. 5 shows the denoised images of  
 629 a scene captured by Canon 5D Mark 3 at ISO = 3200. We  
 630 can see that CBM3D, NC, NI and CC would either remain  
 631 noise or generate artifacts, while TNRD, “WNNM1”, and  
 632 “WNNM2” over-smooth much the image. By using the pro-  
 633

648

649

650

651

652

653

654

655

656

657

658

659

660

661

662

663

664

665

666

667

668

669

670

671

672

673

674

675

676

677

678

679

680

681

682

683

684

685

686

687

688

689

690

691

692

693

694

695

696

697

698

699

700

701

702

703

704

705

706

707

708

709

710

711

712

713

714

715

716

717

718

719

720

721

722

723

724

725

726

727

728

729

730

731

732

733

734

735

736

737

738

739

740

741

742

743

744

745

746

747

748

749

750

751

752

753

754

755

Table 1. PSNR(dB) results of different denoising algorithms on 24 natural images.

Image#	$\sigma_r = 40, \sigma_g = 20, \sigma_b = 30$								
	CBM3D	MLP	TNRD	NI	NC	WNNM0	WNNMI	WNNM2	MC-WNNM
1	25.24	25.70	25.74	23.85	24.90	26.01	25.95	25.58	<b>26.66</b>
2	28.27	30.12	30.21	25.90	25.87	30.08	30.11	29.80	<b>30.20</b>
3	28.81	31.19	31.49	26.00	28.58	31.58	31.61	31.20	<b>32.25</b>
4	27.95	29.88	29.86	25.82	25.67	30.13	30.16	29.84	<b>30.49</b>
5	25.03	26.00	26.18	24.38	25.15	26.44	26.39	25.32	<b>26.82</b>
6	26.24	26.84	26.90	24.65	24.74	27.39	27.30	26.88	<b>27.98</b>
7	27.88	30.28	30.40	25.63	27.69	30.47	30.54	29.70	<b>30.98</b>
8	25.05	25.59	25.83	24.02	25.30	26.71	26.75	25.26	<b>26.90</b>
9	28.44	30.75	30.81	25.94	27.44	30.86	30.92	30.29	<b>31.49</b>
10	28.27	30.38	30.57	25.87	28.42	30.65	30.68	29.95	<b>31.26</b>
11	26.95	28.00	28.14	25.32	24.67	28.19	28.16	27.61	<b>28.63</b>
12	28.76	30.87	31.05	26.01	28.37	30.97	31.06	30.58	<b>31.48</b>
13	23.76	23.95	23.99	23.53	22.76	24.27	24.15	23.52	<b>24.89</b>
14	26.02	26.97	27.11	24.94	25.68	27.20	27.15	26.55	<b>27.57</b>
15	28.38	30.15	30.44	26.06	28.21	30.52	30.60	30.13	<b>30.81</b>
16	27.75	28.82	28.87	25.69	26.66	29.27	29.21	29.02	<b>29.96</b>
17	27.90	29.57	29.80	25.85	28.32	29.78	29.79	29.16	<b>30.40</b>
18	25.77	26.40	26.41	24.74	25.70	26.63	26.56	26.01	<b>27.22</b>
19	27.30	28.67	28.81	25.40	26.52	29.19	29.22	28.67	<b>29.57</b>
20	28.96	30.40	30.76	24.95	25.90	30.79	30.83	29.97	<b>31.07</b>
21	26.54	27.53	27.60	25.06	26.48	27.80	27.75	27.12	<b>28.34</b>
22	27.05	28.17	28.27	25.36	26.60	28.21	28.16	27.81	<b>28.64</b>
23	29.14	32.31	32.51	26.13	23.24	31.89	31.97	31.21	<b>32.34</b>
24	25.75	26.41	26.53	24.55	25.73	27.10	27.03	26.18	<b>27.59</b>
Average	27.13	28.54	28.68	25.24	26.19	28.84	28.83	28.22	<b>29.31</b>

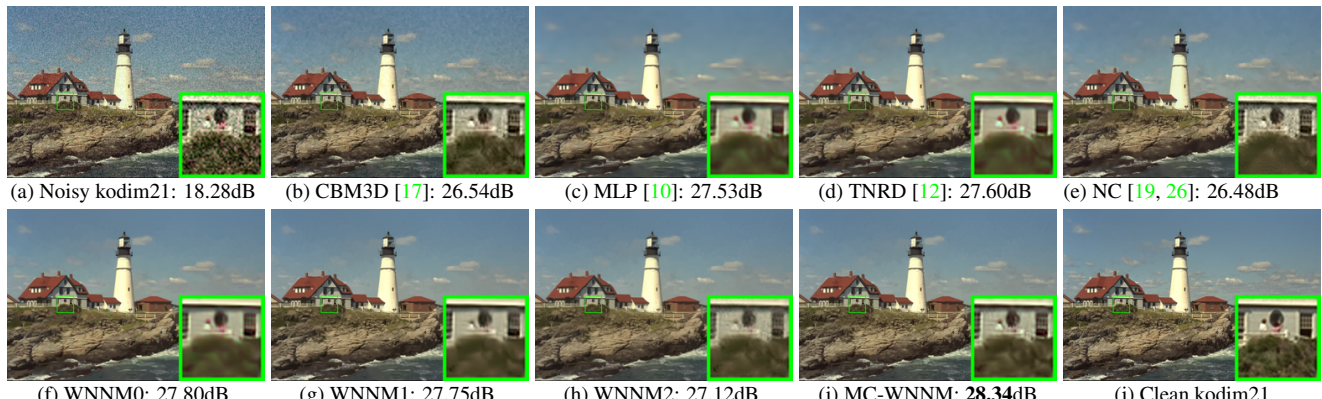
Figure 3. Denoised images of different methods on the image "kodim21" degraded by AWGN with different standard derivations of  $\sigma_r = 40, \sigma_g = 20, \sigma_b = 30$  on R, G, B channels, respectively. The images are better to be zoomed in on screen.

Figure 4. The 15 cropped real noisy images used in [14].

posed MC-WNNM model achieves better visual quality results than other methods. More visual comparisons can be found in the supplementary files.

## 5. Conclusion and Future Work

The real noisy images have different noise structures among the R, G, B channels due to the preprocessing steps of the digital camera pipelines in CCD or CMOS sensors. This makes the real image denoising problem much more complex than grayscale image denoising. In this paper, we proposed a novel multi-channel (MC) model for real color image denoising. By introducing a weighting matrix to the concatenated weighted nuclear norm minimization (WNNM) model, the proposed MC-WNNM model can process adaptively the different noise structures in each of the R, G, B channels and exploit the non-local self similarity property of natural images. Though no longer having closed-form solution, we successfully solved the MC-WNNM model via an ADMM algorithm by reformulating the MC-WNNM model as a linear equality-constrained

Table 2. PSNR(dB) results of different methods on 15 cropped real noisy images used in [14].

Camera Settings	CBM3D	MLP	TNRD	NI	NC	CC	WNNM0	WNNM1	WNNM2	MC-WNNM
Canon 5D Mark III ISO = 3200	39.76	39.00	39.51	35.68	36.20	38.37	37.51	39.74	39.98	<b>41.13</b>
	36.40	36.34	36.47	34.03	34.35	35.37	33.86	35.12	36.65	<b>37.28</b>
	36.37	36.33	36.45	32.63	33.10	34.91	31.43	33.14	34.63	<b>36.52</b>
Nikon D600 ISO = 3200	34.18	34.70	34.79	31.78	32.28	34.98	33.46	35.08	35.08	<b>35.53</b>
	35.07	36.20	36.37	35.16	35.34	35.95	36.09	36.42	36.84	<b>37.02</b>
	37.13	39.33	39.49	39.98	40.51	<b>41.15</b>	39.86	40.78	39.24	39.56
Nikon D800 ISO = 1600	36.81	37.95	38.11	34.84	35.09	37.99	36.35	38.28	38.61	<b>39.26</b>
	37.76	40.23	40.52	38.42	38.65	40.36	39.99	41.24	40.81	<b>41.43</b>
	37.51	37.94	38.17	35.79	35.85	38.30	37.15	38.04	38.96	<b>39.55</b>
Nikon D800 ISO = 3200	35.05	37.55	37.69	38.36	38.56	<b>39.01</b>	38.60	39.93	37.97	38.91
	34.07	35.91	35.90	35.53	35.76	36.75	36.04	37.32	37.30	<b>37.41</b>
	34.42	38.15	38.21	40.05	40.59	39.06	39.73	<b>41.52</b>	38.68	39.39
Nikon D800 ISO = 6400	31.13	32.69	32.81	34.08	34.25	34.61	33.29	<b>35.20</b>	34.57	34.80
	31.22	32.33	32.33	32.13	32.38	33.21	31.16	33.61	33.43	<b>33.95</b>
	30.97	32.29	32.29	31.52	31.76	33.22	31.98	33.62	<b>34.02</b>	33.94
Average	35.19	36.46	36.61	35.33	35.65	36.88	35.77	37.27	37.12	<b>37.71</b>

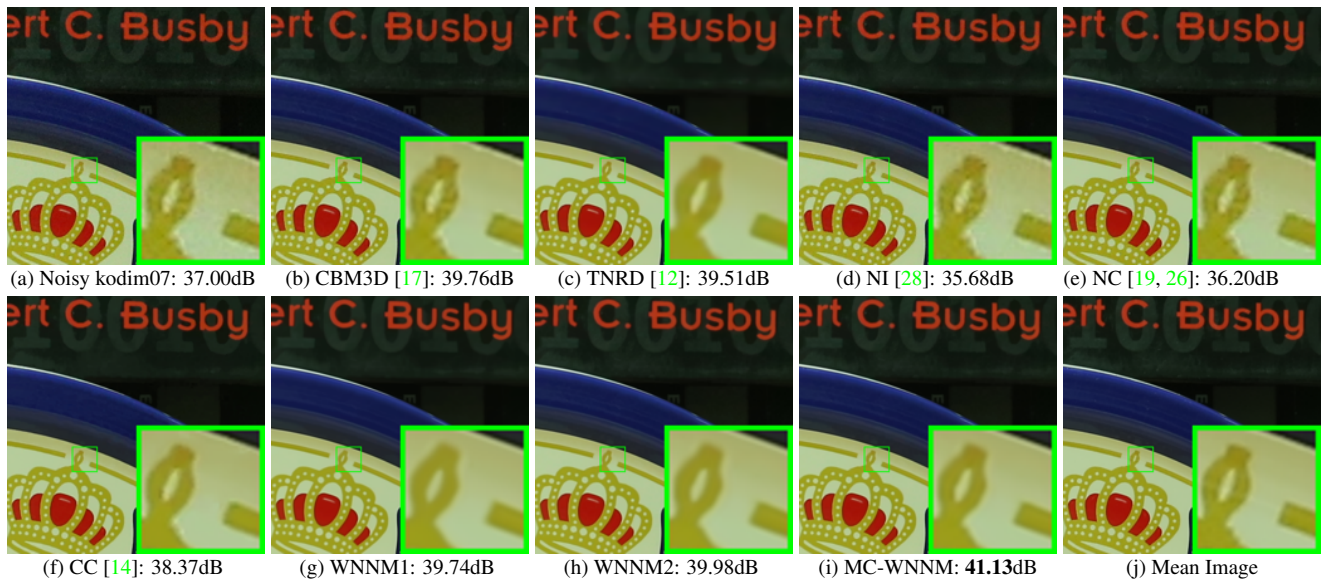


Figure 5. Denoised images of a region cropped from the real noisy image “Canon 5D Mark 3 ISO 3200 1” [14] by different methods. The images are better to be zoomed in on screen.

problem with two separable variables. We also studied the convergence property of the ADMM algorithm. Extensive experiments on synthetic and real color image denoising demonstrate that, the proposed MC-WNNM model outperforms the other competing denoising methods on both synthetic color noisy images as well as real-world noisy images. Introducing a weighting matrix to the traditional models for grayscale image denoising can boost the performance of traditional models on color image denoising tasks. We believe that this work can be extended in at least two directions. Firstly, the weighting matrix beyond the diagonal form, such as correlation form [31], may bring better performance on color image denoising. Secondly, the proposed MC-WNNM model can be further extended to deal with hyperspectral images, which may contain hundreds of channels (bands) with different noise structures in different

channels.

## References

- [1] A. Buades, B. Coll, and J. M. Morel. A non-local algorithm for image denoising. *IEEE Conference on Computer Vision and Pattern Recognition (CVPR)*, pages 60–65, 2005. **1**
- [2] K. Dabov, A. Foi, V. Katkovnik, and K. Egiazarian. Image denoising by sparse 3-D transform-domain collaborative filtering. *IEEE Transactions on Image Processing*, 16(8):2080–2095, 2007. **1, 2**
- [3] M. Elad and M. Aharon. Image denoising via sparse and redundant representations over learned dictionaries. *IEEE Transactions on Image Processing*, 15(12):3736–3745, 2006. **1, 2**
- [4] J. Mairal, F. Bach, J. Ponce, G. Sapiro, and A. Zisserman.

- 864 Non-local sparse models for image restoration. *IEEE International Conference on Computer Vision (ICCV)*, pages 918  
865 2272–2279, 2009. 919  
866  
867  
868 [5] W. Dong, L. Zhang, G. Shi, and X. Li. Nonlocally centralized sparse representation for image restoration. *IEEE Transactions on Image Processing*, 22(4):1620–1630, 2013. 920  
869  
870  
871 [6] J. Xu, L. Zhang, W. Zuo, D. Zhang, and X. Feng. Patch group based nonlocal self-similarity prior learning for image 921  
872 denoising. *IEEE International Conference on Computer Vision (ICCV)*, pages 244–252, 2015. 922  
873  
874  
875 [7] S. Gu, L. Zhang, W. Zuo, and X. Feng. Weighted nuclear 923  
876 norm minimization with application to image denoising. *IEEE Conference on Computer Vision and Pattern 924  
877 Recognition (CVPR)*, pages 2862–2869, 2014. 1, 2, 5  
878  
879 [8] S. Roth and M. J. Black. Fields of experts. *International 925  
880 Journal of Computer Vision*, 82(2):205–229, 2009. 1  
881  
882 [9] D. Zoran and Y. Weiss. From learning models of natural 926  
883 image patches to whole image restoration. *IEEE International Conference on Computer Vision (ICCV)*, pages 927  
884 479–486, 2011. 928  
885  
886 [10] H. C. Burger, C. J. Schuler, and S. Harmeling. Image 929  
887 denoising: Can plain neural networks compete with BM3D? *IEEE Conference on Computer Vision and Pattern 930  
888 Recognition (CVPR)*, pages 2392–2399, 2012. 5, 6, 7  
889  
890  
891 [11] U. Schmidt and S. Roth. Shrinkage fields for effective 931  
892 image restoration. *IEEE Conference on Computer Vision and 932  
893 Pattern Recognition (CVPR)*, pages 2774–2781, June 2014. 933  
894  
895 [12] Y. Chen, W. Yu, and T. Pock. On learning optimized 934  
896 reaction diffusion processes for effective image restoration. *IEEE Conference on Computer Vision and Pattern 935  
897 Recognition (CVPR)*, pages 5261–5269, 2015. 1, 5, 6, 7, 8  
898  
899 [13] B. Leung, G. Jeon, and E. Dubois. Least-squares luma- 936  
900 chroma demultiplexing algorithm for bayer demosaicking. *IEEE Transactions on Image Processing*, 20(7):1885–1894, 937  
901 2011. 1, 2  
902  
903 [14] S. Nam, Y. Hwang, Y. Matsushita, and S. J. Kim. A holistic 938  
904 approach to cross-channel image noise modeling and its 939  
905 application to image denoising. *IEEE Conference on Computer 940  
906 Vision and Pattern Recognition (CVPR)*, pages 1683–1691, 941  
907 2016. 1, 2, 5, 6, 7, 8  
908  
909 [15] H. C. Karaimer and M. S. Brown. A software platform for 942  
910 manipulating the camera imaging pipeline. *European Conference 943  
911 on Computer Vision (ECCV)*, October 2016. 1  
912  
913 [16] Julien Mairal, Michael Elad, and Guillermo Sapiro. Sparse 944  
914 representation for color image restoration. *IEEE Transactions on Image Processing*, 17(1):53–69, 2008. 1, 2  
915  
916  
917 [17] K. Dabov, A. Foi, V. Katkovnik, and K. Egiazarian. Color 945  
918 image denoising via sparse 3D collaborative filtering with 919  
919 grouping constraint in luminance-chrominance space. *IEEE 920  
921  
922  
923  
924  
925  
926  
927  
928  
929  
930  
931  
932  
933  
934  
935  
936  
937  
938  
939  
940  
941  
942  
943  
944  
945  
946  
947  
948  
949  
950  
951  
952  
953  
954  
955  
956  
957  
958  
959  
960  
961  
962  
963  
964  
965  
966  
967  
968  
969  
970  
971* International Conference on Image Processing (ICIP), pages 313–316, 2007. 1, 2, 5, 6, 7, 8  
920  
921  
922  
923  
924  
925  
926  
927  
928  
929  
930  
931  
932  
933  
934  
935  
936  
937  
938  
939  
940  
941  
942  
943  
944  
945  
946  
947  
948  
949  
950  
951  
952  
953  
954  
955  
956  
957  
958  
959  
960  
961  
962  
963  
964  
965  
966  
967  
968  
969  
970  
971 Conference on Computer Vision and Pattern Recognition (CVPR), June 2016. 1, 2  
920  
921  
922  
923  
924  
925  
926  
927  
928  
929  
930  
931  
932  
933  
934  
935  
936  
937  
938  
939  
940  
941  
942  
943  
944  
945  
946  
947  
948  
949  
950  
951  
952  
953  
954  
955  
956  
957  
958  
959  
960  
961  
962  
963  
964  
965  
966  
967  
968  
969  
970  
971 Found. Trends Mach. Learn., 3(1):1–122, January 2011. 1  
920  
921  
922  
923  
924  
925  
926  
927  
928  
929  
930  
931  
932  
933  
934  
935  
936  
937  
938  
939  
940  
941  
942  
943  
944  
945  
946  
947  
948  
949  
950  
951  
952  
953  
954  
955  
956  
957  
958  
959  
960  
961  
962  
963  
964  
965  
966  
967  
968  
969  
970  
971 Generalized singular value thresholding. *AAAI*, 2015. 1  
920  
921  
922  
923  
924  
925  
926  
927  
928  
929  
930  
931  
932  
933  
934  
935  
936  
937  
938  
939  
940  
941  
942  
943  
944  
945  
946  
947  
948  
949  
950  
951  
952  
953  
954  
955  
956  
957  
958  
959  
960  
961  
962  
963  
964  
965  
966  
967  
968  
969  
970  
971 SIAM Journal on Optimization, 20(4):1956–1982, 2010. 2  
920  
921  
922  
923  
924  
925  
926  
927  
928  
929  
930  
931  
932  
933  
934  
935  
936  
937  
938  
939  
940  
941  
942  
943  
944  
945  
946  
947  
948  
949  
950  
951  
952  
953  
954  
955  
956  
957  
958  
959  
960  
961  
962  
963  
964  
965  
966  
967  
968  
969  
970  
971 International Journal of Computer Vision, pages 1–26, 2016. 2, 3, 4, 5, 6  
920  
921  
922  
923  
924  
925  
926  
927  
928  
929  
930  
931  
932  
933  
934  
935  
936  
937  
938  
939  
940  
941  
942  
943  
944  
945  
946  
947  
948  
949  
950  
951  
952  
953  
954  
955  
956  
957  
958  
959  
960  
961  
962  
963  
964  
965  
966  
967  
968  
969  
970  
971 Psychometrika, 1(3):211–218, 1936. 2  
920  
921  
922  
923  
924  
925  
926  
927  
928  
929  
930  
931  
932  
933  
934  
935  
936  
937  
938  
939  
940  
941  
942  
943  
944  
945  
946  
947  
948  
949  
950  
951  
952  
953  
954  
955  
956  
957  
958  
959  
960  
961  
962  
963  
964  
965  
966  
967  
968  
969  
970  
971 The noise clinic: a blind image denoising algorithm. <http://www.ipol.im/pub/art/2015/125/>. Accessed 01 28, 2015. 2, 5, 6, 7, 8  
920  
921  
922  
923  
924  
925  
926  
927  
928  
929  
930  
931  
932  
933  
934  
935  
936  
937  
938  
939  
940  
941  
942  
943  
944  
945  
946  
947  
948  
949  
950  
951  
952  
953  
954  
955  
956  
957  
958  
959  
960  
961  
962  
963  
964  
965  
966  
967  
968  
969  
970  
971 Bayesian non-local means filter, image redundancy and adaptive dictionaries for noise removal. *International Conference on Scale Space and Variational Methods in Computer Vision*, pages 520–532, 2007. 2  
920  
921  
922  
923  
924  
925  
926  
927  
928  
929  
930  
931  
932  
933  
934  
935  
936  
937  
938  
939  
940  
941  
942  
943  
944  
945  
946  
947  
948  
949  
950  
951  
952  
953  
954  
955  
956  
957  
958  
959  
960  
961  
962  
963  
964  
965  
966  
967  
968  
969  
970  
971 Neatlab ABSsoft. Neat Image. <https://ni.neatvideo.com/home>. 2, 5, 6, 8  
920  
921  
922  
923  
924  
925  
926  
927  
928  
929  
930  
931  
932  
933  
934  
935  
936  
937  
938  
939  
940  
941  
942  
943  
944  
945  
946  
947  
948  
949  
950  
951  
952  
953  
954  
955  
956  
957  
958  
959  
960  
961  
962  
963  
964  
965  
966  
967  
968  
969  
970  
971 Single-image noise level estimation for blind denoising. *IEEE Transactions on Image Processing*, 22(12):5226–5237, 2013. 5  
920  
921  
922  
923  
924  
925  
926  
927  
928  
929  
930  
931  
932  
933  
934  
935  
936  
937  
938  
939  
940  
941  
942  
943  
944  
945  
946  
947  
948  
949  
950  
951  
952  
953  
954  
955  
956  
957  
958  
959  
960  
961  
962  
963  
964  
965  
966  
967  
968  
969  
970  
971 An efficient statistical method for image noise level estimation. *IEEE International Conference on Computer Vision (ICCV)*, December 2015. 5, 6  
920  
921  
922  
923  
924  
925  
926  
927  
928  
929  
930  
931  
932  
933  
934  
935  
936  
937  
938  
939  
940  
941  
942  
943  
944  
945  
946  
947  
948  
949  
950  
951  
952  
953  
954  
955  
956  
957  
958  
959  
960  
961  
962  
963  
964  
965  
966  
967  
968  
969  
970  
971 Computing the nearest correlation matrix problem from finance. *IMA Journal of Numerical Analysis*, 22(3):329, 2002. 8  
920  
921  
922  
923  
924  
925  
926  
927  
928  
929  
930  
931  
932  
933  
934  
935  
936  
937  
938  
939  
940  
941  
942  
943  
944  
945  
946  
947  
948  
949  
950  
951  
952  
953  
954  
955  
956  
957  
958  
959  
960  
961  
962  
963  
964  
965  
966  
967  
968  
969  
970  
971